Conjugated Bile Acid Hydrolase Is a Tetrameric N-Terminal Thiol Hydrolase with Specific Recognition of Its Cholyl but Not of Its Tauryl Product[†,‡]

Maksim Rossocha,[§] Robert Schultz-Heienbrok,[*,§] Holger von Moeller,[§] James P. Coleman,[||] and Wolfram Saenger[§]

Freie Universität Berlin, Institut für Kristallographie, Takustrasse 6, 14195 Berlin, Germany, and Department of Microbiology and Immunology, East Carolina University, Greenville, North Carolina 27858

Received December 21, 2004; Revised Manuscript Received February 22, 2005

ABSTRACT: Bacterial bile salt hydrolases catalyze the degradation of conjugated bile acids in the mammalian gut. The crystal structures of conjugated bile acid hydrolase (CBAH) from *Clostridium perfringens* as apoenzyme and in complex with taurodeoxycholate that was hydrolyzed to the reaction products taurine and deoxycholate are described here at 2.1 and 1.7 Å resolution, respectively. The crystal structures reveal close relationship between CBAH and penicillin V acylase from *Bacillus sphaericus*. This similarity together with the N-terminal cysteine classifies CBAH as a member of the N-terminal nucleophile (Ntn) hydrolase superfamily. Both crystal structures show an identical homotetrameric organization with dihedral (D_2 or 222) point group symmetry. The structure analysis of *C. perfringens* CBAH identifies critical residues in catalysis, substrate recognition, and tetramer formation which may serve in further biochemical characterization of bile acid hydrolases.

Conjugated bile acids are common in mammals and consist of glycine or taurine linked by an amide bond to cholesterol-based bile acids (Figure 1). Bile salt (acid) hydrolases (BSH[1]) catalyzing the hydrolysis of this amide bond are expressed in many bacterial genera that reside in the mammalian intestine, among them *Clostridium perfringens* and the commercially popular "probiotic" bifidobacterium strains (*1*). Within the intestine, BSH active bacterial strains regulate the delicate balance of the cholesterol enterohepatic recirculation by competing for bile acids with the active reuptake in the terminal ileum (*2*, *3*), thereby effectively lowering serum cholesterol levels (*4*). Although the biological function of BSH enzymes is not well-understood, they have received much attention because they are used to quantify secreted bile acids in biological fluids and because they play a role in human (patho)physiology. Deconjugated bile salts have been implicated in formation of gallstones (*5*) and colorectal cancer (*6*), and BSH active bacterial strains have been administered orally to intervene in cholesterol circulation (*7*).

Conjugated bile acid hydrolase (CBAH) from *C. perfringens* [EC 3.5.1.24] was first shown in 1967 to have catalytic activity toward glycyl- and taurocholic acids (*8*). The enzyme was purified (*9*), and the gene encoding CBAH was cloned, sequenced, and shown to be homologous to penicillin V acylase (PVA) from *Bacillus sphaericus* (*10*), of which the three-dimensional structure has been determined (*11*). On the basis of sequence homology, it has been suggested that CBAH belongs to the superfamily of N-terminal nucleophile (Ntn)-hydrolases which are characterized by a conserved $\alpha\beta\beta\alpha$-folding pattern and by autocatalytic cleavage of N-terminal residues to expose an N-terminal nucleophile amino acid (*12*, *13*). Despite their common structural and catalytic features, the Ntn-hydrolases have evolved beyond any recognizable sequence homology and comprise enzymes as diverse as the proteasome subunits, lysosomal aspartylglucosaminidase, glutamine PRPP amidotransferase, and the commercially important enzyme penicillin G acylase which is used to produce the starting material for semisynthetic penicillins.

We have determined the structure of CBAH from *C. perfringens* in order to discover key residues of the active site and of the substrate binding pocket. This is of interest both for further characterization of the Ntn-hydrolase superfamily and for understanding the substrate selectivity of bacterial BSH enzymes.

Here, we present the 2.1 Å resolution structure of unliganded *C. perfringens* CBAH apoenzyme and the 1.7 Å resolution crystal structure of the complex formed between CBAH and the substrate taurodeoxycholic acid (Figure 1) that was hydrolyzed to the reaction products deoxycholate and taurine. The tertiary structure and the presence of cysteine2 as an N-terminal nucleophile confirm that this CBAH belongs to the Ntn-hydrolase superfamily and, in particular, to the penicillin V acylase family. In agreement with biochemical studies, CBAH is a tetramer displaying D_2 (222) point group symmetry in both crystal forms. In addition

[†] This work was supported by a grant from the Deutsche Forschungsgemeinschaft and by Fonds der Chemischen Industrie.

[‡] PDB entries for apoCBAH and tauroCBAH are 2bjg and 2bjf, respectively.

* To whom correspondence should be addressed. Institut für Kristallographie, FU Berlin, Takustr.6, 14195, Berlin, Germany. Phone, 0049-30-83853456; fax, 0049-30-83856702; e-mail, rsh@chemie.fu-berlin.de.

[§] Freie Universität Berlin.

[||] East Carolina University.

[1] Abbreviations: apoCBAH, CBAH apoenzyme; BSH, bile salt hydrolase; CA, cephalosporin acylase; CBAH, conjugated bile acid hydrolase; DCA, deoxycholate; DTT, dithiothreitol; EDTA, ethylendiamin-tetraacetate; IPTG, isopropyl-β-D-thiogalactopyranoside; Ntn, N-terminal nucleophile; PGA, penicillin G acylase; PVA, penicillin V acylase; tauroCBAH, CBAH in complex with the reaction products taurine and deoxycholate.

10.1021/bi0473206 CCC: $30.25
Published on Web 03/25/2005

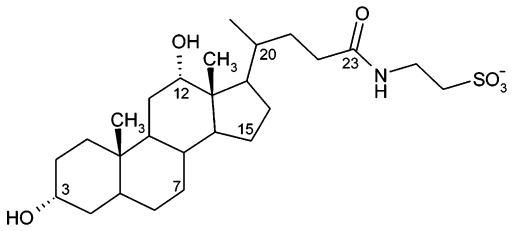

FIGURE 1: Chemical structure of taurodeoxycholate.

to active site residues previously described in Ntn-hydrolases, we have found Arg18 to play a potentially essential role in catalytic functioning of the enzyme. Substrate specificity is conferred by a hydrophobic pocket that recognizes the cholyl moiety of the substrate, whereas the amino acid moiety is not specifically recognized.

MATERIALS AND METHODS

Cloning, Overexpression, and Purification. Subcloning the *cbah* gene from *C. perfringens* into the pKK233-2 plasmid was described earlier (*10*). The plasmids were transformed into *Escherichia coli* BL21 DE3 (Invitrogen), and cells were grown in Luria−Bertani medium at 37 °C throughout. After expression was induced at $A_{600} = 0.8$ with 200 μM IPTG, cells were allowed to grow for another 4 h before harvesting and resuspending in 25 mM Hepes (pH 7.5), 10 mM DTT, 25 mM NaCl, and 5 mM EDTA. After cell lysis (French Press) and centrifugation, the protein in the supernatant was purified as described (*10*) with some modifications. The Hepes buffer was exchanged overnight against a NaAcetate buffer at pH 4.5 and subsequently centrifuged. The supernatant was used for ammonium sulfate precipitation (45%). The pellet was discarded, and the supernatant was adjusted to 100 mM phosphate (pH 6.0), 1.8 M ammonium sulfate, 10 mM DTT, and 5 mM EDTA and subjected to hydrophobic interaction chromatography (Poros 20PE, Applied Biosystems), using a linear gradient from 1.8 to 0 M ammonium sulfate. Finally, fractions containing *C. perfringens* CBAH were collected, concentrated, and applied to a size-exclusion column (Superdex 200, Amersham Bioscience) equilibrated with 10 mM NaAcetate (pH 5.5), 400 mM NaCl, 1 mM DTT, 1 mM EDTA, and 10% (v/v) glycerol resulting in a homogeneous protein solution as confirmed by SDS gel analysis. For crystallization trials, the protein solution was supplemented with 10 mM DTT and concentrated to 15 mg/mL as quantified by a Bradford assay (*14*). The apoenzyme was crystallized from a protein batch that did not contain DTT.

Crystallization. Crystallization was achieved by vapor diffusion at 18 °C. The CBAH−product complex was crystallized in hanging drops by mixing 3 μL of protein solution and 2 μL of reservoir solution. The reservoir solution contained 2.6 M ammonium sulfate, 100 mM NaCitrate, pH 6.0, and 1 mM taurodeoxycholate (Acros Organics). The apoCBAH crystals were grown in sitting drops by mixing 1.5 μL of protein solution and 1 μL of reservoir solution. The reservoir solution contained 25% PEG 4000, 200 mM ammonium sulfate, and 100 mM Bis-Tris, pH 5.5. Both the orthorhombic complex and the tetragonal apoenzyme crystals appeared within 3 days.

Data Collection, Processing, Structure Determination, and Refinement. All X-ray diffraction data were collected at 100 K at the Protein Structure Factory beamline BL14.2 of Free University Berlin at BESSY (Berlin, Germany) using a wavelength of 0.9776 Å. Prior to cryocooling, the mother liquor of the tetragonal/apoenzyme crystal (apoCBAH) was replaced by reservoir solution containing 25% ethylene glycol, and the mother liquor of the orthorhombic crystals (tauroCBAH) was replaced by reservoir solution containing 20% (v/v) glycerol. The data sets were recorded with a MAR 345 imaging plate detector system and processed using the programs DENZO and SCALEPACK (*15*). Details of the data collection statistics are summarized in Table 1.

Table 1: Data Collection and Refinement Statistics

	data collection	
	tauroCBAH	apoCBAH
space group	*F*222	$P4_122$
cell dimensions (Å)	88.85, 90.84, 188.55	63.16, 63.16, 339.38
molecules/asym unit	1	2
resolution range (Å)	50−1.67	50−2.1
unique reflections	42911	34729
completeness overall (%)	97.1	81.1
overall ($I/(\sigma(I))$)	29.4 (7.8)	19 (8.4)
overall R_{sym}	3.8 (11.7)	7.2 (16.5)
data redundancy	3.6	5.6
	refinement	
resolution range (Å)	50−1.67	50−2.1
R-factor	17.7	20.0
R_{free}	19.5	24.6
protein atoms	2676	5216
rmsd		
bond length (Å)	0.006	0.008
bond angles (deg)	1.026	1.040
Average *B*-factor (Å^2)	14.84	30.19
main chains	12.97	29.89
side chains	16.32	30.49
Ramachandran plot (% residues)		
favorable regions	90.5	91.0
allowed region	8.8	8.3
generously allowed region	0.7	0.3
disallowed region	0	0.3

The tauroCBAH structure was determined by molecular replacement using data between 3.5 and 30 Å with the program Phaser (*16*, *17*). A poly-serine model of penicillin V acylase monomer (PDB ID 3pva, chain A) was taken as a search model. The molecular replacement solution could be further improved automatically with the program ARP/wARP (*18*, *19*). Composite omit maps calculated with the CNS software package (*20*) were used for manual model building in O (*21*). Refinement of individual loops was achieved using the simulated annealing protocol from the CNS software package. Finally, the whole model was subjected to restrained refinement using REFMAC (*22*). The products taurine and deoxycholate were built manually into the electron density using O. The model was then alternately refined and manually rebuilt in O until convergence of the conventional *R*-factor and of *R*free. Five percent of the data were reserved for cross-validation. Water molecules were added using the automated refinement program ARP in concert with REFMAC.

The tetragonal crystal structure of the apoCBAH was determined using the refined model of the tauroCBAH structure as a search model input for MOLREP (*23*). Subsequent steps were carried out as described above for the CBAH−product structure except that tight NCS constraints for the two molecules in the asymmetric unit were applied during the early steps of refinement which were later

relaxed. Detailed refinement statistics are presented in Table 1.

Structure Analysis and Generation of Figures. The stereochemistry of the models was analyzed with the programs PROCHECK (*24*) and WHATCHECK (*25*). All atomic coordinate superpositions were carried out with the program LSQKAP (*26*). Structural alignments were done using the Dali server (*27*, *28*). The amino acid sequence alignment was calculated with the program BioEdit developed by T. A. Hall. The CCP4 program suite (*29*) was used to calculate crystal contacts (CONTACT) and buried surface areas (AREAIMOL).

The topography diagram was created with the aid of the program TOPS (*30*). The schematic drawing of the deoxycholate binding site was generated with the aid of the program LIGPLOT (*31*). The omit map was calculated using the CNS software package (*20*). Figures 2, 3, 4A, 4B, and 6 were generated using the programs MolScript (*32*) and Raster3D (*33*) with the help of the graphical user interface MOLDRAW developed by N. Sträter.

RESULTS

Overall Structure. Two crystal structures of *C. perfringens* CBAH, recombinantly expressed in *E. coli*, were determined. The apoenzyme (apoCBAH) crystallized in the tetragonal space group $P4_122$ with two monomers (apoA and apoB) in the asymmetric unit, whereas CBAH in complex with taurodeoxycholate (tauroCBAH) crystallized in the orthorhombic space group *F*222 with one monomer in the asymmetric unit. Before and/or during crystallization, taurodeoxycholate was hydrolyzed to the products taurine and deoxycholate that are both found in the crystal structure.

The structures were determined by molecular replacement and refined to crystallographic *R*/*R*free-factors of 20.0/24.6 and 17.7/19.5 at 2.1 and 1.7 Å resolution, respectively. Both models contain the full polypeptide chain with only the initial formyl-methionine missing, in agreement with N-terminal sequencing and MALDI-TOF spectra (not shown), yielding a molecular mass of 37 060 Da for the 328 amino acids long polypeptide. In the apoCBAH (molecules apoA and apoB) and the tauroCBAH models the ϕ, φ torsion angles of all residues are found in allowed regions of the Ramachandran plot, and only Glu135 and Thr174 lie in the additionally allowed regions but are clearly defined in the electron density. The ϕ, φ torsion angles of Thr174 are located in the α_L region, and those of Glu135 are located between regions typical for α-helices and β-strands of the Ramachandran plot. Both amino acids are located in loop segments, Glu135 in the deoxycholate binding site between β10 and β11 and Thr174 next to Asn175 in the active site, between β13 and α3.

Since apoCBAH was purified and crystallized without DTT, the SH-group of Cys2 was partially oxidized as shown in the electron density, whereas tauroCBAH was treated throughout under reducing conditions using DTT and crystallized in the native form. Both structures do not differ significantly from each other, and consequently, the structure of tauroCBAH, that has the higher resolution and better refinement statistics, is described below unless stated otherwise.

The CBAH monomer is made up of a single globular domain with approximate dimensions of 40 Å × 50 Å × 55 Å excluding one extended loop (200s loop) from Gln188 to Pro225 which stretches out for about 40 Å (Figure 2A). Including the β-sheet of this extended loop, the domain has a six-layered structure of composition $\beta\alpha\beta\beta\alpha\beta$ (Figure 2B). The core of the protein is composed of two sandwiched antiparallel β-sheets that contain N- and C-termini and are covered by a layer of antiparallel α-helices. The N-terminal β-sheet (I) is made up of five antiparallel β-strands with topography NH_2-β1-β2-β16-β17-β18, and the C-terminal β-sheet (II) is composed of eight antiparallel β-strands with topography β13-β12-β11-β8-β7-β6-β3-β19-COOH, the last five β-strands being packed in parallel fashion against β-sheet I. The product deoxycholate is primarily bound to residues from β-sheet II located on strands β6, β7, and β11.

This $\alpha\beta\beta\alpha$ fold together with the fact that the first amino acid is cleaved off to expose the potentially catalytic Cys2 residue classifies CBAH as a member of the Ntn-hydrolase superfamily (*12*, *13*, *34*). An additional characteristic of this group of enzymes is that they all display higher quaternary structural organization which has also been found in the here studied CBAH structure.

Quaternary Structure. Both apo- and tauroCBAH form homotetramers in the crystal structures. Moreover, they both have the same intratetramer contacts but completely different crystal contacts, associated with orthorhombic and tetragonal space groups. Since crystallization was achieved under slightly acidic conditions (pH 6.0 and 5.5, respectively) near the catalytic optimum of the enzyme (5.8−6.4, (*9*)), our data show that CBAH exists as a homotetramer with dihedral symmetry under physiological conditions.

Besides the extended 200s loop with antiparallel β-strands β14 and β15, β-strands β9 and β17−β19 as well as the α-helices α3−α7 and the turns and loops connecting these strands and helices are the contact sites for the tetramer organization of CBAH (Figure 3). This configuration leaves the substrate binding pocket (formed by β6, β7, and β11) freely accessible to solvent.

The subunits in the CBAH tetramer are related by dihedral (D_2 or 222) point group symmetry that is clearly different from a 4-fold (C_4) symmetry (Figure 3B). The dihedral organization results in different contacts between the individual protomers. The largest interface within the tetramer is the one observed between molecules A and C or B and D, respectively, that are related by the horizontal 2-fold rotation axis 2_H in Figure 3B. This dimer interface has a buried surface area of 3167 Å^2 per protomer with 38 amino acids per protomer involved in contact formation. The interface contains residues from the long C-terminal tail, helices α4−α7, strands β17−β19, and part of the 200s loop.

The second largest interface is formed between molecules A and B or C and D, respectively, that are related by the perpendicular 2-fold rotational symmetry axis 2_P in Figure 3B. This contact involves helices α3−α5 and, in particular, a β-sheet (β14, β15) of the 200s loop and involves 21 amino acids with a total buried surface area of 1405 Å^2 per protomer. In the tetramer, the four 200s loops cross over the symmetry center leading to an extensively interlocked oligomer. The third interface, formed by molecules A and D or B and C respectively, that are related by the vertical 2-fold rotation axis 2_V in Figure 3B, is a minor contact site involving only eight residues that are located mostly on α3 and on the N-terminus of α5 and buries a surface area of

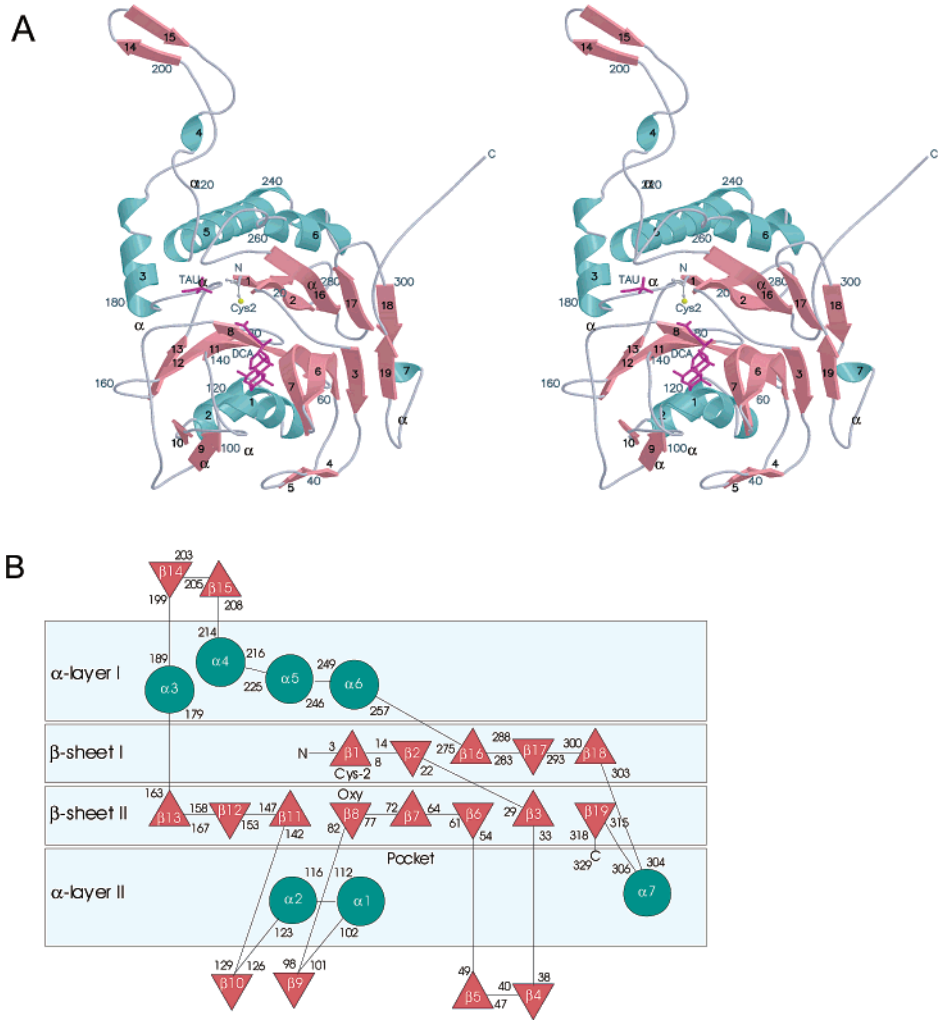

FIGURE 2: Overall structural features of *C. perfringens* CBAH. The reaction products taurine and deoxycholate are shown in magenta. (A) Stereodiagram of CBAH monomer. (B) Topography of CBAH monomer.

490 Å^2 per protomer. These buried surface areas in the homotetramer add up to 5062 Å^2 for each protomer, but since there is some overlap, the actually found buried surface amounts to 4934 Å^2 per monomer. The large surface between molecules A−C and B−D suggests that the tetramer may be considered as consisting of two homodimers.

Superposition of apo- and tauroCBAH crystal structures did not reveal any significant conformational differences between monomers, the overall root-mean-square deviations being not more than 0.36 Å between C_α atoms of monomers as well as tetramers of both crystal forms. This agrees with kinetic data of BSH enzymes that fit the Michaelis−Menten equation (*8*, *9*, *35*), and suggest that CBAH may be described as an enzyme with four independent catalytic sites showing no cooperativity.

Substrate Binding Pocket and Active Site. Although the structure of CBAH complexed with taurine and deoxycholate includes only the reaction products and not the substrate taurodeoxycholate, the catalytically active residues can be inferred from biochemical experiments and from analogy to the active sites of other Ntn-hydrolases (*36*−*39*) showing that Cys2Sγ is involved in catalysis (*40*) (Figure 4A). All residues within the active site and in the substrate binding pocket occupy well-defined positions in the crystal structure.

In the binding pocket, deoxycholate is sandwiched by Phe61 and Ile137 on the side of the deoxycholyl ring A and by Met20, Ala68, and Phe26 on the side of the isovaleric acid side chain of deoxycholate (Figure 4, parts B and C). Additional important hydrophobic interactions are formed between Ile133 and deoxycholyl ring B and Leu142 and ring D. The only hydrogen bonds (below 3.4 Å) are donated by Cys2Sγ and Arg18Nη2 to deoxycholate O26 and by H_2O127 to O25. There are long hydrogen bonds between Thr140 and both O12 and O3 and between Tyr24 and O12. Table 2 lists the main contacts along with their respective *B*-factors between cholate and protein side chains. Clear electron density was found for deoxycholate, whereas the density for the taurine is less well-defined. This is also reflected in their average temperature factors as the *B*-value for taurine is 55.5 Å^2 and, for cholate, 28.8 Å^2. Since the amino acids contacting the reaction products have a mean *B*-value of ~15 Å^2, it is even likely that the relatively high *B*-factor for deoxycholate indicates incomplete occupancy rather than high mobility.

Interestingly, taurine has a "reversed" orientation pointing with its sulfo group toward Cys2 and leaving the active site with its amino group ahead. Compared to cholate, the electron density around taurine is less well-defined. The weak electron density and high *B*-values of taurine are indicative of a significant disorder and/or lower occupation of this ligand, in agreement with the finding that taurine forms only one hydrogen bond to a protein side chain (the sulfo oxygen O1S to Asn82Nδ2 and is mainly solvent-exposed (Table 2).

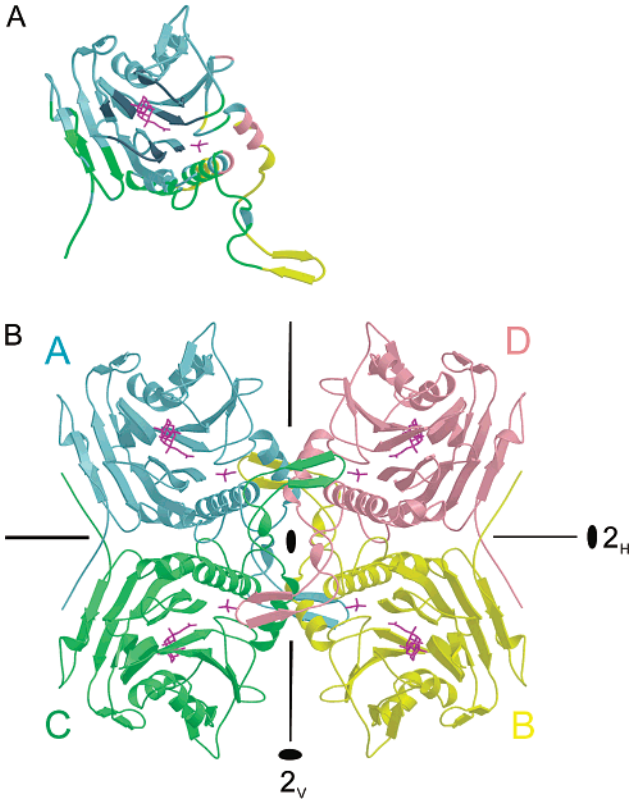

FIGURE 3: Tetramer formation of CBAH. Reaction products taurine and deoxycholate are indicated in stick presentation. (A) Ribbon diagram of CBAH monomer. Contact surfaces with other molecules in the tetramer indicated by color-coding as in panel B. The shown monomer has the same orientation as protomer A in panel B. (B) CBAH homotetramer with monomers colored differently. Twofold rotation axes in the paper plane marked 2_H (horizontal) and 2_V (vertical), and the one perpendicular (normal) to the paper plane (2p) is indicated by the black ellipse in the center.

Another hydrogen bond to O3S is formed by Gln212Nϵ2 of a symmetry-related CBAH molecule. Both the involvement of a symmetry-related molecule in the coordination of taurine and its positional disorder make it impossible to decide whether the reversed orientation of taurine has any meaning in the dissociation of this product from the protein.

In the active site, Cys2Sγ is well-positioned for nucleophilic attack on the amide bond of conjugated bile acids lying in a position defined by the products deoxycholate and taurine. Together with Arg18Nη2, Cys2Sγ hydrogen-bonds to deoxycholate O26 that is well-defined in the electron density. After attack of Cys2Sγ on the taurodeoxycholate amide carbon, a likely oxyanion hole for stabilization of the negatively charged carbonyl oxygen in the tetrahedral intermediate is formed by a peptide NH of Asn82 on the β8 opposite the catalytic center and Asn175Nδ2 in the loop connecting β13 and α3. Both N−H groups are 4 Å away from the catalytic Sγ and 3.5 Å apart from each other. Asp21 is well-positioned to stabilize the catalytic base (α-amino group of nucleophile Cys2 (*12*, *41*, *42*)) during the reaction (Figure 4A). Arg228 on α5 is close to the catalytic Cys2 and forms hydrogen bonds to peptide O of Cys2 and Asn175Oδ1. From the structure, it is not clear whether this apparent stabilization of the active site geometry is the only function of Arg228, but arginines are conserved in equivalent positions in all described Ntn-hydrolases (Figure 6) and have been shown to be necessary for catalytic function (*41*, *43*, *44*). According to our model, Arg18 could also play a role in catalysis as it is well-positioned to stabilize a negatively charged Cys2Sγ prior to nucleophilic attack. Arg18 is 3.4 Å away from the catalytic Sγ in tauroCBAH and apoCBAH and hydrogen-bonded to deoxycholate O26 in tauroCBAH (Figure 4C).

DISCUSSION

Structural Comparison to Other Proteins. Ntn-hydrolases are characterized by a four-layered catalytically active $\alpha\beta\beta\alpha$-structure where the two core β-sheets are antiparallel and packed against each other (*12*, *13*, *45*). Besides this common fold, they all catalyze amide bonds through an autocatalytically exposed N-terminal nucleophile (*34*, *46*−*48*) that might be a Ser, Thr, or Cys, with the N-terminal amino group functioning as base in the reaction (*12*, *41*, *42*). Although this group of enzymes seems to have a common mechanism of action, they differ considerably in their substrate specificities.

The crystal structure of *C. perfringens* CBAH reveals a close structural and catalytic similarity to Ntn-hydrolases. Not only does the overall topography with the typical $\alpha\beta\beta\alpha$-core classify the protein as belonging to this group, but also the N-terminal f-Met was found to be cleaved off to expose Cys2 which resides in the active center. Structural comparison to known structures deposited in the Protein Data Bank using Dali (*28*) underlines the relationship of *C. perfringens* CBAH to Ntn-hydrolases (Table 3). Among the 10 significantly similar structures (*Z*-score $\geq$ 2), the first nine all classify as Ntn-hydrolases. Not surprisingly, *C. perfringens* CBAH resembles penicillin acylase from *B. sphaericus* (PVA) most closely with which it shares the highest sequence homology. The similarities also extend to the quaternary structures of the proteins. For PVA, a similar tetramer formation with dihedral symmetry has been described (*11*). The similarity in tetramer formation between CBAH and PVA is also reflected in the high number of strictly conserved residues found at the tetramer contact sites (see Figure 5 and discussion below). There is overall high structural similarity with modest, low, or even absent sequence conservation among the members of the Ntn-hydrolase superfamily (*12*).

An interesting observation is the structural similarity to Ser/Thr phosphatase C2 which is a member of the metallophosphoesterase superfamily that shares a similar fold to Ntn-hydrolases with an $\alpha/\beta-\alpha-\beta-\beta-\alpha$ layered structure. As in the case of Ntn-hydrolases, the active site is located between the core β-strands. It remains to be seen whether this coincidence is due to a distantly homologous relationship or emerged by convergent evolution toward a particularly stable fold.

To uncover the most critical residues in tetramer formation, we have matched the monomer−monomer contact sites in *C. perfringens* CBAH with a sequence alignment of BSH enzymes and penicillin V acylase (Figure 5). The smallest contact interface between molecules A and B in the tetramer (Figure 3) has only two highly conserved residues, Trp181 and Asn185 (Figure 5), that form a four-side chains minicluster where Trp181 contacts Asn185 and vice versa. Besides its contact to Asn185, Trp181 stacks hydrophobically with the Trp181 of the neighboring mol-

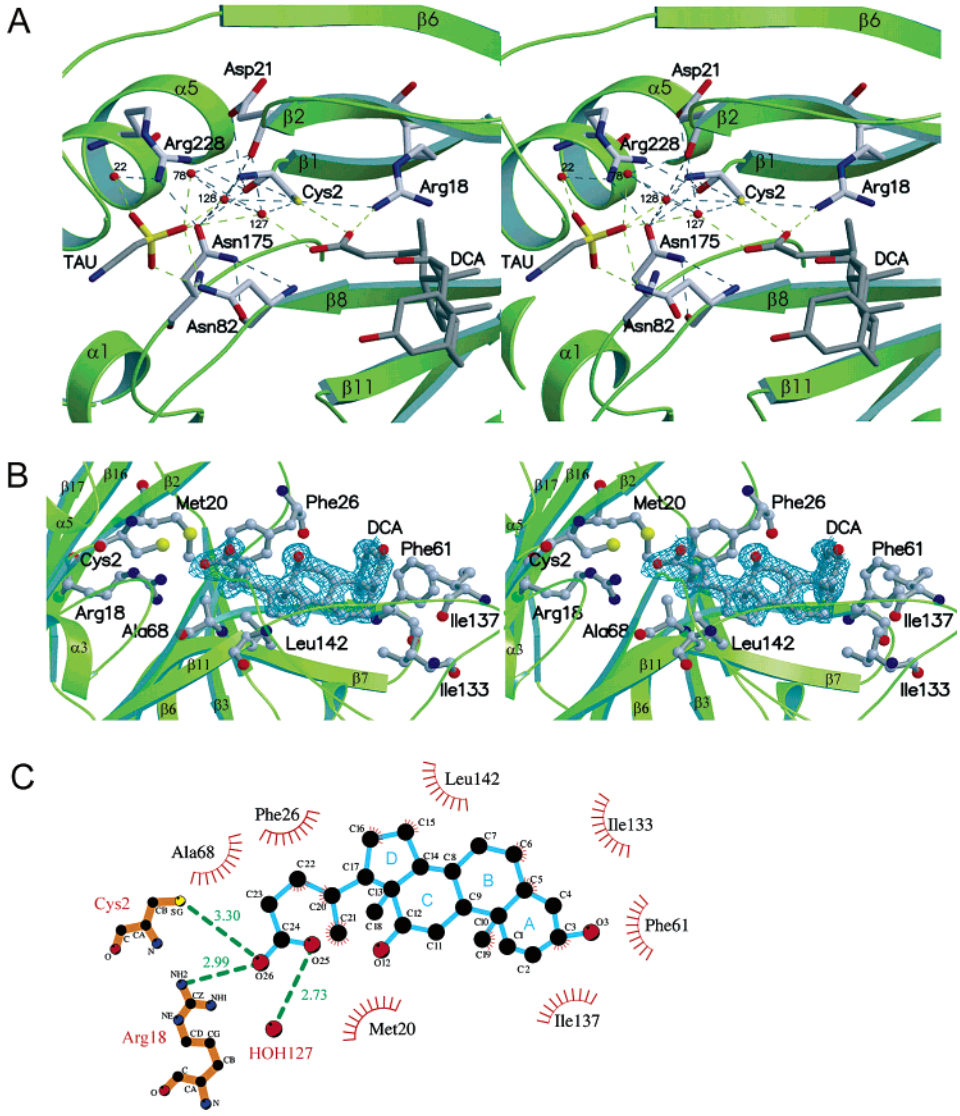

FIGURE 4: Active site and substrate binding pocket of CBAH. (A) Residues of the active site with the products taurine (TAU) and deoxycholate (DCA). Hydrogen bonds between the products and the protein are shown in green, all other hydrogen bonds are gray. (B) Main contacts between deoxycholate and the protein residues. Density around deoxycholate from a $2F_o - F_c$ composite omit map contoured at 1σ level shown in blue. (C) Schematic drawing of diagram B.

ecule. In some species, Trp181 is replaced by phenylalanine or tyrosine which can form equivalent contacts. Most of the highly conserved residues of the interface A−B are in the 200s loop, Leu186, Leu207, and Gly218 in molecule A contacting residues Leu186, Leu207, and Gly218 in molecule B, respectively. The reciprocal nature of most of the contacts between the conserved residues of the dimer interface supports the view that conservation is due to contact formation. The large interface between molecules A and C comprises 10 strictly or highly conserved residues including a cluster from Gly218 to Asp222 making again reciprocal contacts to the same residues of the neighboring molecule. Additional highly conserved residues that make reciprocal contacts are His254, Tyr294, and Ile299. The contact residues of Gly213 and Gly264 are not as well-conserved as the glycines themselves. Since both glycines assume φ/ψ angles that cannot be easily formed by other residues (110.4°/13.1° and 103.5°/−28.8° respectively), it is likely that conservation of these glycines is essential for the course of the main chain rather than for contact formation.

Conservation of the Active Site. It has long been known that cysteine is involved in the catalytic function of *C. perfringens* CBAH (*8*, *9*), and recently, the homologous BSH from *Bifidobacterium longum* could be inactivated by a single base substitution Cys1 → Ala (*49*), and the more conservative substitutions Cys1 → Ser and Cys1 → Thr inactivated BSH from *Bifidobacterium bifidum* (*40*). Further residues of the active site have been identified by sequence alignments of penicillin V acylase (PVA) with BSH (*49*), and active site residues in PVA have been identified by comparison with penicillin G acylase (*11*), of which enzyme−inhibitor complexes have been described (*36*). Besides Cys2, residues Asp21, Asn82, Asn175, and Arg228 have been identified as catalytically important in BSHs (Figure 5). PVA uses the same catalytic residues except for Asn82 which is replaced by Tyr82. This, however, does not alter the nature of the active site since only the peptide NH atoms of both residues are important in catalysis by providing an electron acceptor to form the oxyanion hole together with Asn175Nδ2.

Table 2: Main Contacts between Ligands and CBAH Residues[a]

CBAH		ligand		
atom	*B*-value (Å^2)	atom	*B*-value (Å^2)	distance (Å)
		Deoxycholate		
Cys-2, Sγ	15.3	O26	29.0	3.30
Arg-18, NH2	10.5	O26	29.0	2.99
Met-20, Cϵ	14.9	C21	28.5	3.68
Phe-26, Cδ1	14.5	C21	29.0	3.86
Phe-26, Cϵ1	14.4	C21	29.0	3.76
Phe-26, Cζ	14.5	C21	29.0	3.69
Phe-61, Cγ	19.3	C19	28.9	3.69
Phe-61, Cδ1	19.6	C19	28.9	3.68
Ala-68, Cβ	11.1	C20	28.5	3.81
Ile-133, Cγ2	18.8	C6	28.9	3.70
Ile-137, Cγ2	21.8	C3	29.2	3.53
Ile-137, Cγ2	18.9	C4	29.0	3.99
Leu-142, Cδ1	13.7	C16	28.6	3.67
HOH-127	32.0	O25	29.3	2.73
		Taurine		
Asn-82, Nδ2	17.6	O1S	55.6	2.81
HOH-22	11.4	O3S	55.4	2.71
HOH-128	26.9	O1S	55.6	2.53
HOH-78	18.7	O1S	55.6	2.58

[a] Contacts with a cutoff of 3.4 Å for hydrogen bonds and a distance of 0.25 Å between the van der Waals surfaces of the atoms for van der Waals interactions.

The structure of *C. perfringens* CBAH confirms these earlier analyses. Since the geometry of the active sites is well-conserved, a similar mechanism might be expected for the individual enzymes. The residues of the active site in CBAH superimpose well on the active sites of other members of the Ntn-hydrolase superfamily (Figure 6) including even (except for residue Arg18) cephalosporin acylase (CA) and penicillin G acylase (PGA). It is of interest that Arg18 in the *C. perfringens* CBAH structure superimposes well with Arg18 from PVA (Figure 6), but the side chains of the equivalent residues point in other directions in the more distantly related proteins PGA and CA, which both feature N-terminal serine instead of cysteine in CBAH and in PVA. Since in all four protein's hydrolysis of the respective substrates results in a carboxyl group to which Arg18 binds in our tauroCBAH model, it is likely that conservation of Arg18 is due to its involvement in catalysis rather than in conferring substrate specificity. Being in the vicinity of Cys2Sγ, one possible role of Arg18 might be to lower the pK_a of the nucleophilic Sγ.

Sequence alignments have suggested earlier that Arg18 of PVA might be involved in catalysis (*50*). Interestingly, in glutamine amidotransferase (*51*) and in glucosamine 6-phosphate synthase (*44*), two other members of the Ntn-hydrolase superfamily that act via a nucleophilic CysSγ, the position of Arg18 is occupied by His70 and His71 respectively, which can fulfill a similar role as Arg18 if they are protonated. Clearly, more experiments are needed to assess the role of Arg18 in the catalytic mechanism of the enzyme, especially as Arg18 is also involved in product binding (Figure 4B).

Binding Pocket and Substrate Selectivity. Currently, there are six proteins described in the PDB that are complexed with a cholyl moiety (1ahi, 1aql, 1ihi, 1o1v, 1ot7, and 1tw4). Superpositions based on the cholyl moiety of each of these proteins and CBAH did not reveal any significant similarity of the binding pockets (data not shown). Likewise, structural comparison of the complete proteins using the Dali server did not reveal any structural similarity between them. This, in concert with the obvious homology to Ntn-hydrolases, suggests that the binding pocket of bile salt hydrolases has evolved convergently.

Bile acids are conjugates between the amino acids taurine or glycine and a cholate derived from cholesterol. The cholate is always hydroxylated on C3 in α position. In addition, the most common hydroxyl substituents are none at all (in lithocholic acid), 12α (indeoxycholic acid), 7α (in chenodeoxycholic acid), 7β (in ursodeoxycholic acid), and 7α and 12α (in cholic acid) (*52*). Together, this results in 10 combinations between differently hydroxylated cholate and the two amino acids. It is conceivable that bile salt hydrolases have evolved to recognize bile acids on both the amino acid and cholate groups.

Kinetic data, however, suggest that these enzymes recognize their substrates predominantly at the amino acid moieties and not at the cholate moieties (*10*, *49*, *53*). Our data explain this broad substrate specificity, as the cholate is bound primarily by hydrophobic interactions and the hydroxyl substituents are not recognized through hydrogen bonds to the enzyme. The only hydrogen bonds between protein and the deoxycholate are to the carboxylate group of the isovaleric acid substituents, O25 and O26 in our case. This is in agreement with earlier experiments using epimerized hydroxyl substituents on cholate that did not influence substrate binding (*54*).

Residues of the active site are strictly conserved in bile acid hydrolases (asterisks in Figure 5). By contrast, however, the residues for substrate recognition (gray in Figure 5) are not particularly conserved, although most amino acid substitutions are conservative. The notable exception is Leu142 that is strictly conserved throughout the species and occurs

Table 3: Comparison of CBAH with Known Protein Structures Using Dali[a]

protein	PDB ID	*Z*-score	rmsd	LALI[b]	LSEQ[c]	% IDE
penicillin V acylase	3pva	42.7	1.9	325	334	34
glutaryl 7-aminocephalosporanic acid acylase	1fm2	15.0	3.4	221	520	13
penicillin amidohydrolase	1ajq-B	14.7	3.2	212	557	11
proteasome	1pma-P	9.8	3.2	157	203	7
structural genomics, unknown function	1kuu-A	8.4	3.9	163	202	7
heat shock locus V	1ned-A	8.0	2.9	141	180	9
glucosamine 6-phosphate synthase	1gdo	2.6	4.2	104	238	9
aspartylglucosamidase	1apy-B	2.5	3.8	95	141	5
glutamine amidotransferase	1ecf-B	2.1	5.9	116	500	8
Ser/Thr Phosphatase 2C	1a6q	2.1	4.7	129	363	5

[a] Only the most similar proteasome subunit has been included in the table. [b] Length of aligned sequence. [c] Total length of sequence.

```
                    *                 *   *
CBH_CP    1   M--CTGLALE TKDGLHLFGR NMDIEYSFNQ SIIFIPRNFK CVNKSNKK-E LTTKYAVLGM GTIFDDYPTF  67
CGH_BA    1   M--CTSLTLE TKNGQHLFAR TMDFTLDMNQ EVIIIPRHYQ WNNITGE--I INTKHATVGM GINHQGRIIM  66
CBH_LP    1   M--CTAITYQ SYNN--YFGR NFDYEISYNE MVTITPRKYP LVFRKVEN-- LDHHYAIIGI TADVESYPLY  64
CBH_LJ    1   M--CTGLRFT DDQGNLYFGR NLDVGQDYGE GVIITPRNYP LPYKF-LD-N TTTKKAVIGM GIVVDGYPSY  66
CBH_LA    1   M--CTGLRFT DDQGNLYFGR NLDVGQDYGE GVIITPRNYP LPYKF-LD-N TTTKKAVIGM GIVVDGYPSY  66
BSH_BB    1   M--CTGVRFS DDEGNMYFGR NLDWSFSYGE TILVTPRGYQ YDYEYGAE-G KSEPNAVIGV GVVMTDRPMY  67
CGH_BL    1   M--CTGVRFS DDEGNTYFGR NLDWSFSYGE TILVTPRGYH YDTVFGAG-G KAKPNAVIGV GVVMADRPMY  67
PVA_BS    1   MLGCSSLSIR TTDDKSLFAR TMDFTMEPDS KVIIVPRNYG IRLLEKENVV INNSYAFVGM GSTDITSPVL  70
                  2                18  21

                    *
CBH_CP   68   ADGMNEKGLG CAGLNFPVYV SYSKEDIEGK TNIPVYNFLL WVLANFSSVE EVKEALKNAN IVDIPISENI  137
CGH_BA   67   ADGVNEAGMT CATLYFPGFA TYSQSIDDNT TNLAPFDFVT WSLTQFNSVK ELKKSVDSIT FLDIPLPDLG  136
CBH_LP   65   YDAMNEKGLC IAGLNFAGYA DYKKYDAD-K VNITPFELIP WLLGQFSSVR EVKKNIQKLN LVNINFSEQL  133
CBH_LJ   67   FDCYNEDGLG IAGLNFPHFA KFSDGPIDGK INIASYEIML WVTQNFTHVS EVKEALKNVN LVNEAINTSF  136
CBH_LA   67   FDCFNEDGLG IAGLNFPHFA KFSDGPIDGK INIASYEIML WVTQNFTKVS DVKEALKNVN LVNEAINSSF  136
BSH_BB   68   FDCANEHGLA IAGLNFPGYA SFAHEPVEGT ENVATFEFPL WVARNFDSVD EVEEALKNVT LVSQVVPGQ-  136
CGH_BL   68   FDCANEHGLA IAGLNFPGYA SFVHEPVEGT ENVATFEFPL WVARNFDSVD EVEEALRNVT LVSQIVPGQ-  136
PVA_BS   71   YDGVNEKGLM GAMLYYATFA TYADEPKKGT TGINPVYVIS QVLGNCVTVD DVIEKLTSYT LLNEANIILG  140
                           82

                                                        *
CBH_CP   138  PNTTLHWMIS DITGKSIVVE QTKE-KLNVF DNNIGVLTNS PTFDWHVANL NQYVGLRYNQ VPEFKLGDQS  206
CGH_BA   137  LTPPLHWILA DKWGDCIVLD PTSE-GLKLY DNPLGVMTNS PEFNWHLQNL RQYIGLKSQP FAPTEWSNLP  205
CBH_LP   134  PLSPLHWLVA DK-QESIVIE SVKE-GLKIY DNPVGVLTNN PNFDYQLFNL NNYRALSNST PQNSFSEKVD  201
CBH_LJ   137  AVAPLHWIIS DS-DEAIIVE VSKQYGMKVF DDKVGVLTNS PDFNWHLTNL GNYTGLNPHD ATAQSWNGQK  205
CBH_LA   137  AVAPLHWIIS DK-DEAIIVE ISKQYGMKVF DDRLGVLTNS PDFNWHLTNL GNYTGLDPHD ATAQSWNGQK  205
BSH_BB   137  QESLLHWFIG DG-TRSIVVE QMAD-GMHVH HDDVDVLTNQ PTFDFHMENL RNYMCVSNEM AEPTTWGKAE  204
CGH_BL   137  QESLLHWFIG DG-KRSIVVE QMAD-GMHVH HDDVDVLTNQ PTFDFHMENL RNYMCVSNEM AEPTSWGKAS  204
PVA_BS   141  FAPPLHYTFT DASGESIVIE PDKT-GITIH RKTIGVMTNS PGYEWHQTNL RAYIGVTPNP PQDIMMGDLD  209
                                                      175

                                *
CBH_CP   207  LTALGQGTGL VGLPGDFTPA SRFIRVAFLR DAMIKNDKDS IDLIEFFHIL NNVAMVRGST RTVEEKSDLT  276
CGH_BA   206  LSAFGQGSGS MGLPGDFTPP SRFVRAAYGK QNIQGIDSEE EGVSALFHIL SNCEVPKGGV ITEEGALDNT  275
CBH_LP   202  LDSYSRGMGG LGLPGDLSSM SRFVRAAFTK LNSLSMQTES GSVSQFFHIL GSVEQQKGLC EVTDGKYEYT  271
CBH_LJ   206  VAPWGVGTGS LGLPGDSIPA DRFVKAAYLN VNYPTAKGEK ANVAKFFNIL KSVAMIKGSV VNDQGKDEYT  275
CBH_LA   206  VAPWGVGTGS LGLPGDSIPA DRFVKAAYLN VNYPTVKGKK ANVAKFFNIL KSVAMIKGSV VNKQGSNEYT  275
BSH_BB   205  LSAWGAGVSM HGIPGDVSSP SRFVRVAYTN THYPQQNNEA ANVSRLFHTL VSVQMVDGMS KMGNGQFERT  274
CGH_BL   205  LTAWGAGVGM HGIPGDVSSP SRFVRVAYTN AHYPQQNDEA ANVSRLFHTL GSVQMVDGMA KMGDGQFERT  274
PVA_BS   210  LTPFGQGAGG LGLPGDFTPS ARFLRVAYWK KYTEKAKNET EGVTNLFHIL SSVNIPKGVV LTNEGKTDYT  279
                                  228

CBH_CP   277  QYTSCMCLEK GIYYYNTYEN NQINAIDMNK ENLDGNEIKT YKYNKTLSIN HVN------ 329
CGH_BA   276  IYTSVMCMES GTYYYHTYDC RQIIAVHLFH ENLDTDEIKA YPFQRKQKIF YEN------ 328
CBH_LP   272  IYSSCCDMDK GVYYYRTYDN SQINSVSLNH EHLDTTELIS YPLRSEAQYY AVN------ 324
CBH_LJ   276  VYTACYSSGS KTYYCNFEDD FELKTYKLDD HTMNSTSLVT Y--------- --------- 316
CBH_LA   276  VYTACYSAAT KTYYCNFEND FELKTYKLDD ETMNADKLIT Y--------- --------- 316
BSH_BB   275  LFTSGYSGKT NTYYMNTYED PAIRSFAMSD FDMDSSELIT AD-------- --------- 316
CGH_BL   275  LFTSGYSSKT NTYYMNTYDD PAIRSYAMAD YDMDSSELIS VAR------- --------- 317
PVA_BS   280  IYTSAMCAQS KNYYFKLYDN SRISAVSLMA ENLNSQDLIT FEWDRKQDIK QLNQVNVMS 338
```

FIGURE 5: Sequence alignment: CBAH from *C. perfringens* (CBH_CP), choloylglycine hydrolase from *Bacillus anthracis* (CGH_BA), CBAH from *Lactobacillus plantarum* (CBH_LP), conjugated bile salt hydrolase from *Lactobacillus johnsonii* (CBH_LJ), conjugated bile salt hydrolase from *Lactobacillus acidophilus* (CBH_LA), bile salt hydolase from *Bifidobacterium bifidum* (BSH_BB), choloylglycine hydrolase from *Bifidobacterium longum* (CGH_BL), and penicillin V acylase from *Bacillus sphaericus* (PVA_BS). The alignment highlights active site residues (marked by black asterisk) and residues of the substrate binding pocket (gray). Conserved residues of the contact sites are color coded according to Figure 3B.

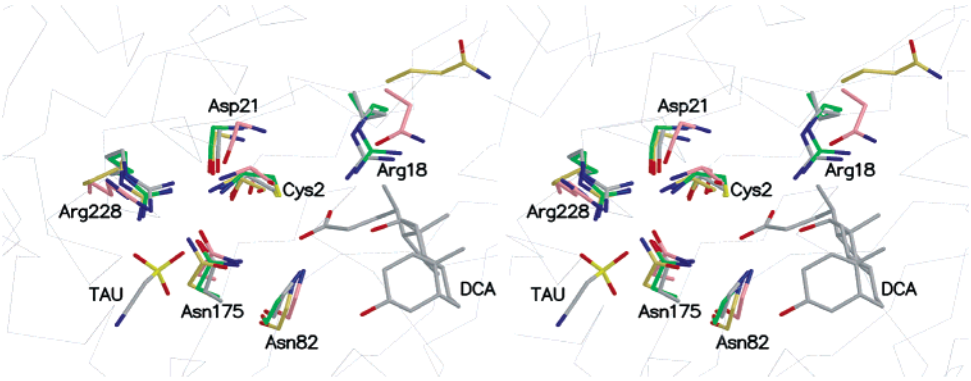

FIGURE 6: Superposition of active site residues (stereodiagram). The superposition is based on the residues listed below with the exception of Arg18 in CBAH (or respective residues in the other proteins). Only main chain atoms of Asn82 and Asp21 are shown. CBAH (gray), Cys2, Arg18, Asp21, Asn82, Asn175, and Arg228; PVA (green), Cys1, Arg17, Asp20, Tyr82, Asn175, and Arg228; CA (yellow), Ser170, Gln189, His192, Val239, Asn413, and Arg443; PGA (pink), Ser1, Asn20, Gln23, Ala69, Asn241, and Arg263. CA, cephalosporin acylase from *Pseudomonas diminuta* (PDB ID 1fm2); PGA, penicillin G acylase from *E. coli* (PDB ID 1gm9); PVA, penicillin V acylase from *Bacillus sphaericus* (PDB ID 3pva).

even in penicillin V acylase which acts on completely different substrates.

Although the substrate specificity of bile salt hydrolases seems to be broad, only small differences have been observed. For example, in CBAH, the K_M values for glycochenodeoxycholic acid and taurocholic acid are in the range of 10^{-2} M, whereas that for deoxy-conjugates is generally in the 10^{-3} M range (*8*), suggesting that CBAH

has a higher affinity toward deoxy-conjugates. Introducing more hydrophilic amino acids in the vicinity of the hydroxyl substituents of the substrates should alter the affinities toward the respective substrates and it should be possible to tailor bile acid hydrolases with any desired bile acid selectivity.

ACKNOWLEDGMENT

We thank Drs. Uwe Müller and Andrew Turnbull for beamtime and support at the FU-Berlin PSF beamline BL14.2 at BESSY, Chengcheng Wang for technical assistance in protein purification and crystallization, and Peter Franke for providing mass spectra.

REFERENCES

1. Tanaka, H., Doesburg, K., Iwasaki, T., and Mierau, I. (1999) Screening of lactic acid bacteria for bile salt hydrolase activity, *J. Dairy Sci. 82*, 2530−2535.
2. Dietschy, J. M. (1974) Bile acids: their absorption from the gastrointestinal tract and role during fat absorption, *Verh. Dtsch. Ges. Inn. Med. 80*, 399−407.
3. Kurz, M., Brachvogel, V., Matter, H., Stengelin, S., Thuring, H., and Kramer, W. (2003) Insights into the bile acid transportation system: the human ileal lipid-binding protein-cholyltaurine complex and its comparison with homologous structures, *Proteins 50*, 312−328.
4. Eyssen, H. (1973) Role of the gut microflora in metabolism of lipids and sterols, *Proc. Nutr. Soc. 32*, 59−63.
5. Thomas, L. A., Veysey, M. J., Bathgate, T., King, A., French, G., Smeeton, N. C., Murphy, G. M., and Dowling, R. H. (2000) Mechanism for the transit-induced increase in colonic deoxycholic acid formation in cholesterol cholelithiasis, *Gastroenterology 119*, 806−815.
6. Singh, J., Hamid, R., and Reddy, B. S. (1997) Dietary fat and colon cancer: modulating effect of types and amount of dietary fat on ras-p21 function during promotion and progression stages of colon cancer, *Cancer Res. 57*, 253−258.
7. De Smet, I., De Boever, P., and Verstraete, W. (1998) Cholesterol lowering in pigs through enhanced bacterial bile salt hydrolase activity, *Br. J. Nutr. 79*, 185−194.
8. Nair, P. P., Gordon, M., and Reback, J. (1967) The enzymatic cleavage of the carbon−nitrogen bond in 3-alpha, 7-alpha, 12-alpha-trihydroxy-5-beta-cholan-24-oylglycine, *J. Biol. Chem. 242*, 7−11.
9. Gopal-Srivastava, R., and Hylemon, P. B. (1988) Purification and characterization of bile salt hydrolase from *Clostridium perfringens*, *J. Lipid Res. 29*, 1079−1085.
10. Coleman, J. P., and Hudson, L. L. (1995) Cloning and characterization of a conjugated bile acid hydrolase gene from *Clostridium perfringens*, *Appl. Environ. Microbiol. 61*, 2514−2520.
11. Suresh, C. G., Pundle, A. V., SivaRaman, H., Rao, K. N., Brannigan, J. A., McVey, C. E., Verma, C. S., Dauter, Z., Dodson, E. J., and Dodson, G. G. (1999) Penicillin V acylase crystal structure reveals new Ntn-hydrolase family members, *Nat. Struct. Biol. 6*, 414−416.
12. Brannigan, J. A., Dodson, G., Duggleby, H. J., Moody, P. C., Smith, J. L., Tomchick, D. R., and Murzin, A. G. (1995) A protein catalytic framework with an N-terminal nucleophile is capable of self-activation, *Nature 378*, 416−419.
13. Oinonen, C., and Rouvinen, J. (2000) Structural comparison of Ntn-hydrolases, *Protein Sci. 9*, 2329−2337.
14. Bradford, M. M. (1976) A rapid and sensitive method for the quantitation of microgram quantities of protein utilizing the principle of protein-dye binding, *Anal. Biochem. 72*, 248−254.
15. Otwinowski, Z., and Minor, W. (1997) Processing of X-ray diffraction data collected in oscillation mode, *Methods Enzymol. 276*, 307−326.
16. Read, R. J. (2001) Pushing the boundaries of molecular replacement with maximum likelihood, *Acta Crystallogr., Sect. D: Biol. Crystallogr. 57*, 1373−1382.
17. Storoni, L. C., McCoy, A. J., and Read, R. J. (2004) Likelihood-enhanced fast rotation functions, *Acta Crystallogr., Sect. D: Biol. Crystallogr. 60*, 432−438.
18. Perrakis, A., Harkiolaki, M., Wilson, K. S., and Lamzin, V. S. (2001) ARP/wARP and molecular replacement, *Acta Crystallogr., Sect. D: Biol. Crystallogr. 57*, 1445−1450.
19. Perrakis, A., Morris, R., and Lamzin, V. S. (1999) Automated protein model building combined with iterative structure refinement, *Nat. Struct. Biol. 6*, 458−463.
20. Brunger, A. T., Adams, P. D., Clore, G. M., DeLano, W. L., Gros, P., Grosse-Kunstleve, R. W., Jiang, J. S., Kuszewski, J., Nilges, M., Pannu, N. S., Read, R. J., Rice, L. M., Simonson, T., and Warren, G. L. (1998) Crystallography & NMR system: a new software suite for macromolecular structure determination, *Acta Crystallogr., Sect. D: Biol. Crystallogr. 54*, 905−921.
21. Jones, T. A., Zou, J. Y., Cowan, S. W., and Kjeldgaard, M. (1991) Improved methods for building protein models in electron-density maps and the location of errors in these models, *Acta Crystallogr., Sect. A 47*, 110−119.
22. Murshudov, G. N., Vagin, A. A., and Dodson, E. J. (1997) Refinement of macromolecular structures by the maximum-likelihood method, *Acta Crystallogr., Sect. D: Biol. Crystallogr. 53*, 240−255.
23. Vagin, A., and Teplyakov, A. (1997) MOLREP: an automated program for molecular replacement, *J. Appl. Crystallogr. 30*, 1022−1025.
24. Laskowski, R. A., Macarthur, M. W., Moss, D. S., and Thornton, J. M. (1993) Procheck—a program to check the stereochemical quality of protein structures, *J. Appl. Crystallogr. 26*, 283−291.
25. Hooft, R. W., Vriend, G., Sander, C., and Abola, E. E. (1996) Errors in protein structures, *Nature 381*, 272.
26. Kabsch, W., Kabsch, H., and Eisenberg, D. (1976) Packing in a new crystalline form of glutamine synthetase from *Escherichia coli*, *J. Mol. Biol. 100*, 283−291.
27. Holm, L., and Sander, C. (1998) Touring protein fold space with Dali/FSSP, *Nucleic Acids Res. 26*, 316−319.
28. Holm, L., and Sander, C. (1993) Protein structure comparison by alignment of distance matrices, *J. Mol. Biol. 233*, 123−138.
29. Bailey, S. (1994) The ccp4 suite—programs for protein crystallography, *Acta Crystallogr., Sect. D: Biol. Crystallogr. 50*, 760−763.
30. Flores, T. P., Moss, D. S., and Thornton, J. M. (1994) An algorithm for automatically generating protein topology cartoons, *Protein Eng. 7*, 31−37.
31. Wallace, A. C., Laskowski, R. A., and Thornton, J. M. (1995) LIGPLOT: a program to generate schematic diagrams of protein−ligand interactions, *Protein Eng. 8*, 127−134.
32. Kraulis, P. J. (1991) Molscript—a program to produce both detailed and schematic plots of protein structures, *J. Appl. Crystallogr. 24*, 946−950.
33. Merritt, E. A., and Murphy, M. E. P. (1994) Raster3d version-2.0—a program for photorealistic molecular graphics, *Acta Crystallogr., Sect. D: Biol. Crystallogr. 50*, 869−873.
34. Saarela, J., Oinonen, C., Jalanko, A., Rouvinen, J., and Peltonen, L. (2004) Autoproteolytic activation of human aspartylglucosaminidase, *Biochem. J. 378*, 363−371.
35. Kirby, L. C., Klein, R. A., and Coleman, J. P. (1995) Continuous spectrophotometric assay of conjugated bile-acid hydrolase, *Lipids 30*, 863−867.
36. Duggleby, H. J., Tolley, S. P., Hill, C. P., Dodson, E. J., Dodson, G., and Moody, P. C. (1995) Penicillin acylase has a single-amino-acid catalytic centre, *Nature 373*, 264−268.
37. Tikkanen, R., Riikonen, A., Oinonen, C., Rouvinen, R., and Peltonen, L. (1996) Functional analyses of active site residues of human lysosomal aspartylglucosaminidase: implications for catalytic mechanism and autocatalytic activation, *EMBO J. 15*, 2954−2960.
38. Oinonen, C., Tikkanen, R., Rouvinen, J., and Peltonen, L. (1995) Three-dimensional structure of human lysosomal aspartylglucosaminidase, *Nat. Struct. Biol. 2*, 1102−1108.
39. Kim, Y., Yoon, K., Khang, Y., Turley, S., and Hol, W. G. (2000) The 2.0 Å crystal structure of cephalosporin acylase, *Structure Fold. Des. 8*, 1059−1068.
40. Kim, G. B., Miyamoto, C. M., Meighen, E. A., and Lee, B. H. (2004) Cloning and characterization of the bile salt hydrolase genes (bsh) from *Bifidobacterium bifidum* strains, *Appl. Environ. Microbiol. 70*, 5603−5612.
41. McVey, C. E., Walsh, M. A., Dodson, G. G., Wilson, K. S., and Brannigan, J. A. (2001) Crystal structures of penicillin acylase enzyme−substrate complexes: structural insights into the catalytic mechanism, *J. Mol. Biol. 313*, 139−150.

42. Kim, J. H., Krahn, J. M., Tomchick, D. R., Smith, J. L., and Zalkin, H. (1996) Structure and function of the glutamine phosphoribosylpyrophosphate amidotransferase glutamine site and communication with the phosphoribosylpyrophosphate site, *J. Biol. Chem. 271*, 15549−1557.
43. Prabhune, A. A., and Sivaraman, H. (1990) Evidence for involvement of arginyl residue at the catalytic site of penicillin acylase from *Escherichia coli*, *Biochem. Biophys. Res. Commun. 173*, 317−322.
44. Isupov, M. N., Obmolova, G., Butterworth, S., Badet-Denisot, M. A., Badet, B., Polikarpov, I., Littlechild, J. A., and Teplyakov, A. (1996) Substrate binding is required for assembly of the active conformation of the catalytic site in Ntn amidotransferases: evidence from the 1.8 Å crystal structure of the glutaminase domain of glucosamine 6-phosphate synthase, *Structure 4*, 801−810.
45. Artymiuk, P. J. (1995) A sting in the (N-terminal) tail, *Nat. Struct. Biol. 2*, 1035−1037.
46. Kim, J. K., Yang, I. S., Rhee, S., Dauter, Z., Lee, Y. S., Park, S. S., and Kim, K. H. (2003) Crystal structures of glutaryl 7-aminocephalosporanic acid acylase: insight into autoproteolytic activation, *Biochemistry 42*, 4084−4093.
47. Kim, Y., Kim, S., Earnest, T. N., and Hol, W. G. (2002) Precursor structure of cephalosporin acylase. Insights into autoproteolytic activation in a new N-terminal hydrolase family, *J. Biol. Chem. 277*, 2823−2829.
48. Li, S., Smith, J. L., and Zalkin, H. (1999) Mutational analysis of *Bacillus subtilis* glutamine phosphoribosylpyrophosphate amidotransferase propeptide processing, *J. Bacteriol. 181*, 1403−1408.
49. Tanaka, H., Hashiba, H., Kok, J., and Mierau, I. (2000) Bile salt hydrolase of *Bifidobacterium longum*—biochemical and genetic characterization, *Appl. Environ. Microbiol. 66*, 2502−2512.
50. Pei, J., and Grishin, N. V. (2003) Peptidase family U34 belongs to the superfamily of N-terminal nucleophile hydrolases, *Protein Sci. 12*, 1131−1135.
51. Smith, J. L., Zaluzec, E. J., Wery, J. P., Niu, L., Switzer, R. L., Zalkin, H., and Satow, Y. (1994) Structure of the allosteric regulatory enzyme of purine biosynthesis, *Science 264*, 1427−1433.
52. Hofmann, A. F., Sjovall, J., Kurz, G., Radominska, A., Schteingart, C. D., Tint, G. S., Vlahcevic, Z. R., and Setchell, K. D. (1992) A proposed nomenclature for bile acids, *J. Lipid Res. 33*, 599−604.
53. Kim, G. B., Yi, S. H., and Lee, B. H. (2004) Purification and characterization of three different types of bile salt hydrolases from Bifidobacterium strains, *J. Dairy Sci. 87*, 258−266.
54. Batta, A. K., Salen, G., and Shefer, S. (1984) Substrate specificity of cholylglycine hydrolase for the hydrolysis of bile acid conjugates, *J. Biol. Chem.* 259, 15035−15039.

BI0473206